Electronic Supplementary Information For

Gaseous Cyclodextrin-*closo*-Dodecaborate Complexes χCD·$[B_{12}X_{12}]^{2-}$ (χ = α, β, γ; X = F, Cl, Br, I): Electronic Structures and Intramolecular Interactions

Yanrong Jiang,[1] Qinqin Yuan,[2] Wenjin Cao,[2] Markus Rohdenburg,[3,4] Marc C. Nierstenhöfer,[5] Zhipeng Li,[1] Yan Yang,[1] Cheng Zhong,[6] Carsten Jenne,[5] Jonas Warneke,[3,7] Haitao Sun,[1,8]* Zhenrong Sun,[1,8]* and Xue-Bin Wang[2]*

[1] *State Key Laboratory of Precision Spectroscopy, School of Physics and Electronic Science, East China Normal University, Shanghai 200062, China*

[2] *Physical Sciences Division, Pacific Northwest National Laboratory, 902 Battelle Boulevard, P.O. Box 999, Richland, Washington 99352, USA*

[3] *Wilhelm-Ostwald-Institut für Physikalische und Theoretische Chemie, Universität Leipzig, 04103 Leipzig, Germany.*

[4] *Institut für Angewandte und Physikalische Chemie, Universität Bremen, Fachbereich 2-Biologie/Chemie, 28359 Bremen, Germany.*

[5] *Fakultät für Mathematik und Naturwissenschaften, Anorganische Chemie, Bergische Universität Wuppertal, Gaußstr. 20, 42119 Wuppertal Germany,*

[6] *College of Chemistry & Molecular Sciences, Wuhan University, Wuhan, Hubei 430072, China*

[7] *Leibniz Institute of Surface Engineering (IOM), Sensoric Surfaces and Functional Interfaces, Permoserstr. 15, D-04318 Leipzig, Germany.*

[8] *Collaborative Innovation Center of Extreme Optics, Shanxi University, Taiyuan, Shanxi 030006, China*

*Corresponding authors: htsun@phy.ecnu.edu.cn (H.-T.S); zrsun@phy.ecnu.edu.cn (Z.-R.S); xuebin.wang@pnnl.gov (X.-B.W.)

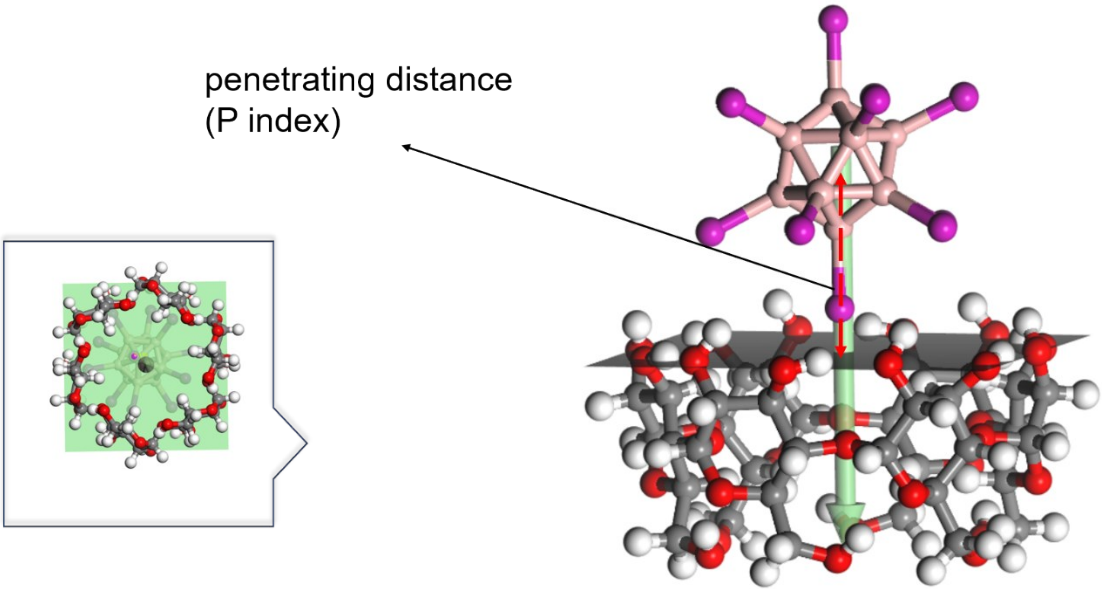

Fig. S1 Schematic diagram for the penetrating distance (P index) between the best fit plane of 2,3-oxygen in CDs for α-CD·$B_{12}I_{12}^{2-}$. The best fit plane of 2,3-oxygen in CDs is defined as the plane possessing the minimum distance between the selected oxygen atoms and the plane employing least square method using Material studio package.[1] Note that for each binding model of CDs·$B_{12}X_{12}^{2-}$ (X = F-I), the penetrating distance between mass-center of $B_{12}X_{12}^{2-}$ (X = F-I) and best fit plane is obtained in Table 2.

def2SVP basis set

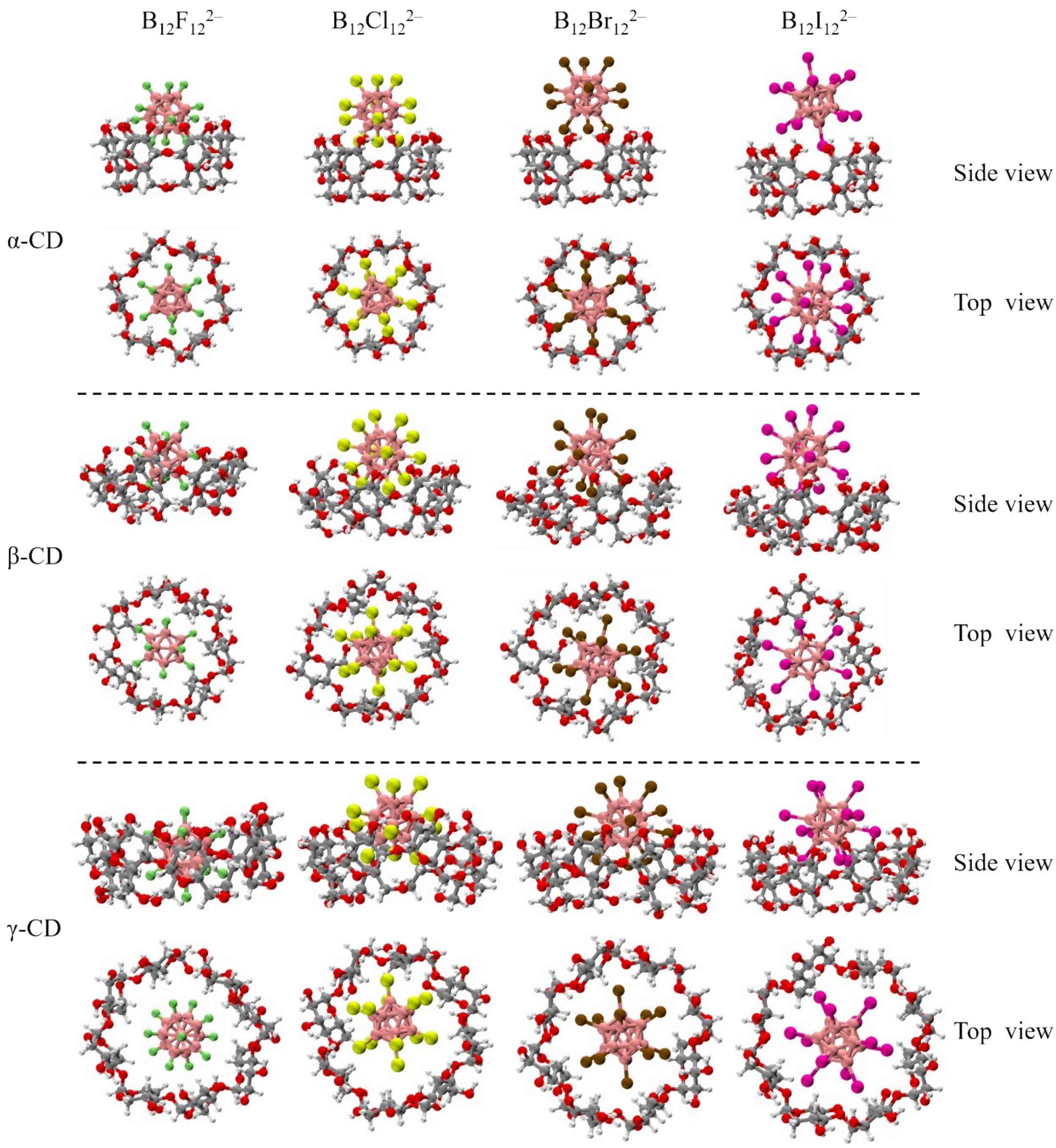

Fig. S2 M06-2X-D3/def2SVP optimized structures of CDs·$B_{12}X_{12}^{2-}$ (X = F-I) with side and top views. Pink, green, yellow, brown, magenta, silver, red, and white balls denote boron (B), fluorine (F), chlorine (Cl), bromine (Br), iodine (I), carbon (C), oxygen (O), hydrogen (H) atoms, respectively. The acting sites of β-CD·$B_{12}F_{12}^{2-}$ changes from three to four by change optimization basis set from def2SVP to TZVP.

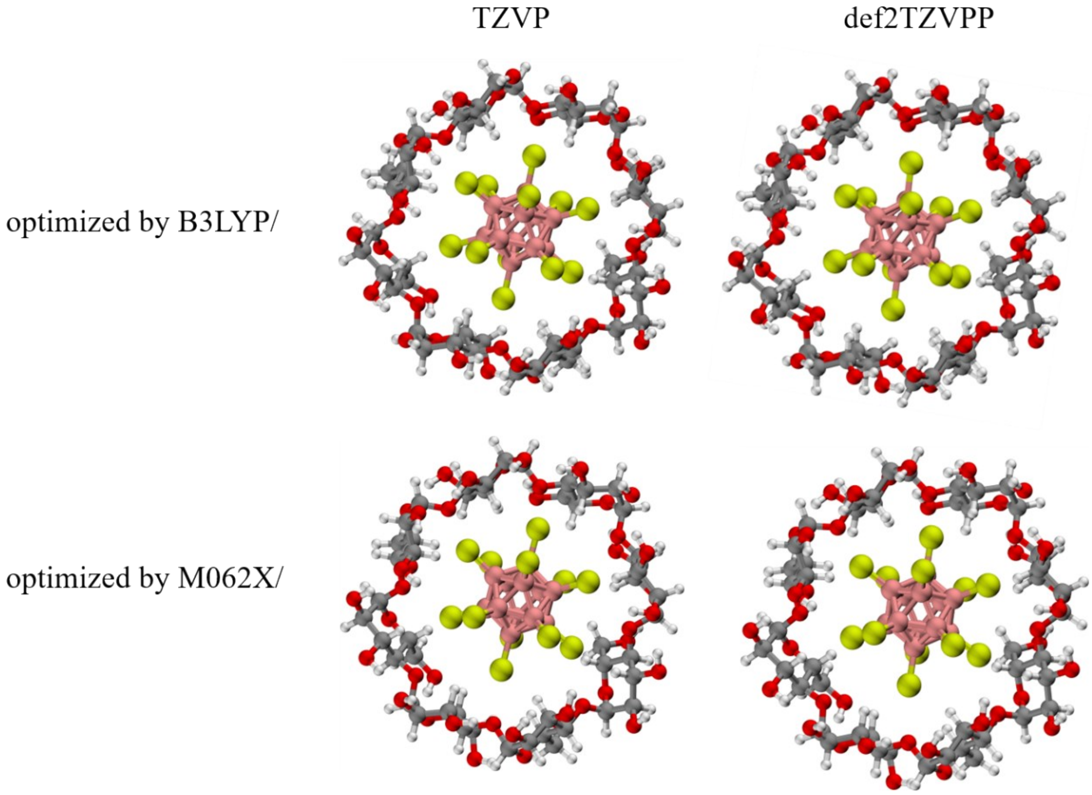

Fig. S3 Structures of γ-CD·$B_{12}Cl_{12}^{2-}$ optimized by M06-2X-D3 and B3LYP-D3(BJ) combined with TZVP and def2TZVPP basis set.

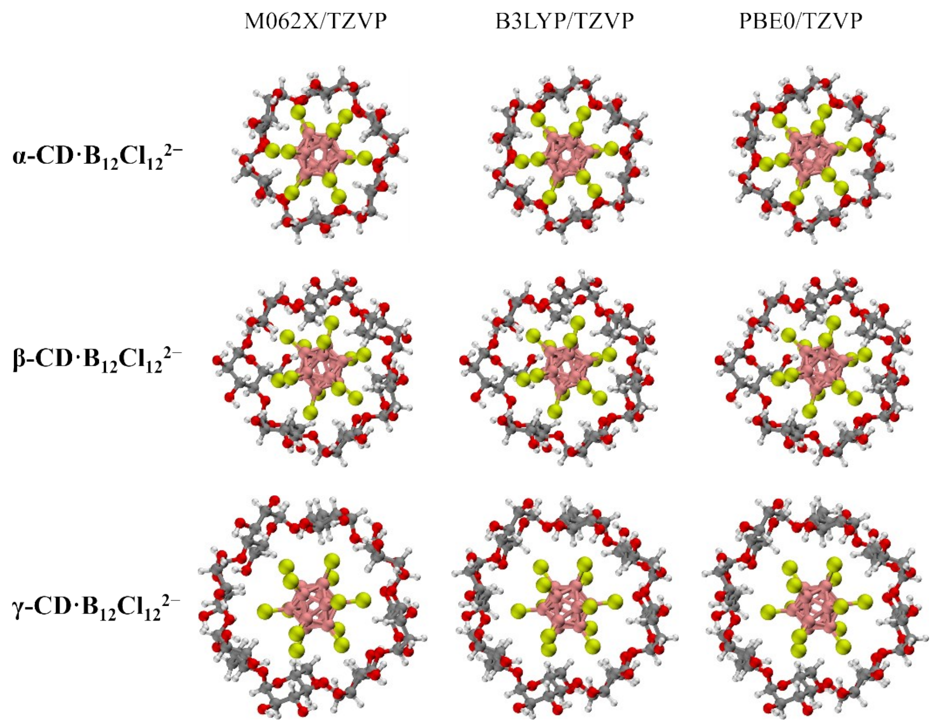

Fig. S4 Optimized geometries of CDs·$B_{12}Cl_{12}^{2-}$ obtained using three different functionals, PBE0+GD3BJ, B3LYP+GD3BJ, M06-2X-D3, all with TZVP basis set.

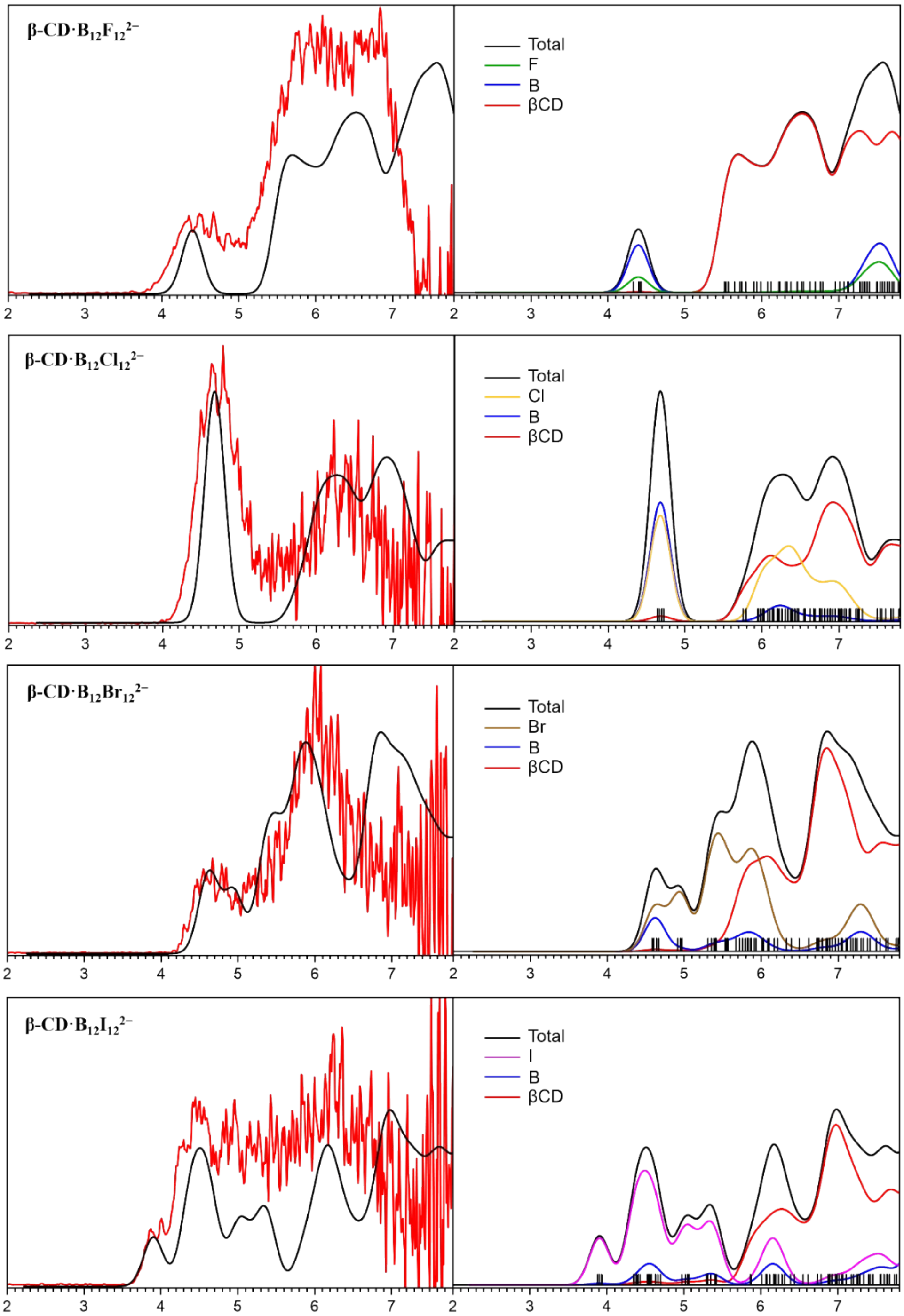

Electron Binding Energies (eV)

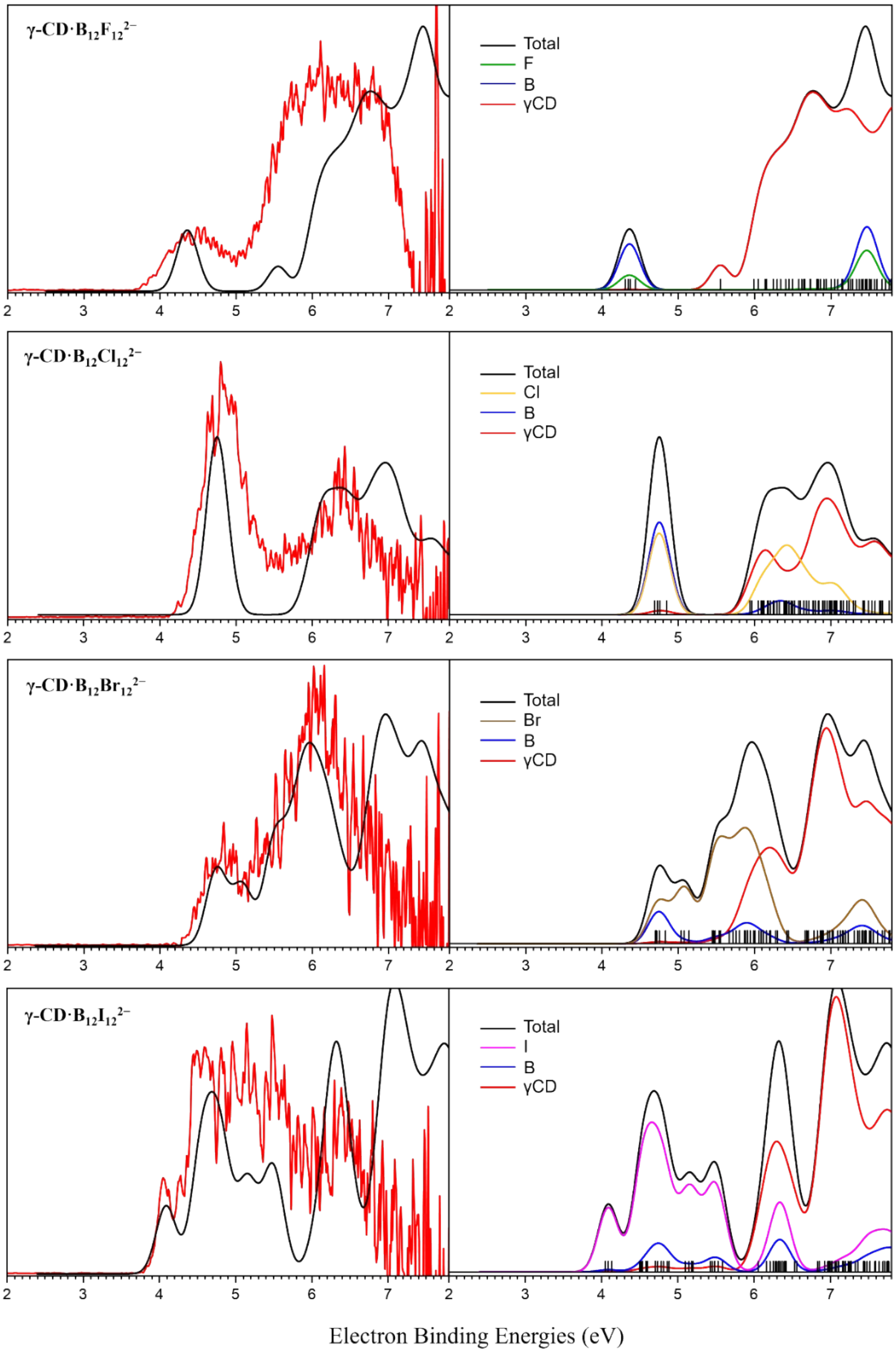

Fig. S5 The measured (left, in red) and simulated (left, in black) NIPE spectra of β-CD/γ-CD·$B_{12}X_{12}^{2-}$ (X = F, Cl, Br and I). The total DOS and partial DOS (right) were plotted with full width at half maxima (FWHM) of 0.30 eV and shifted to allow the HOMO energy fitting the experimental VDE. The measured NIPE spectra of CDs·$B_{12}F_{12}^{2-}$ were derived from reference 3.

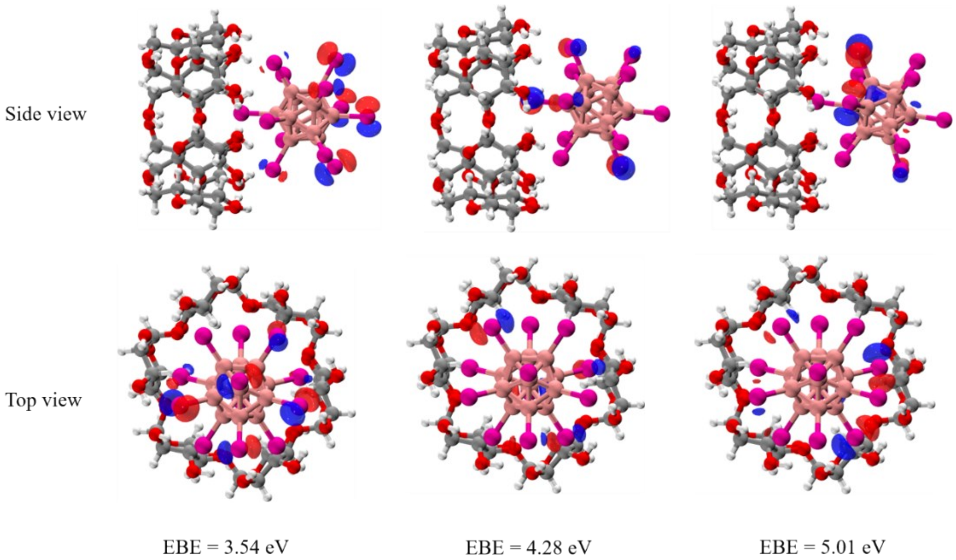

Fig. S6. Plots of occupied molecular orbitals at EBE of 3.54 eV, 4.28 eV, and 5.01 eV for α-CD·$B_{12}I_{12}^{2-}$.

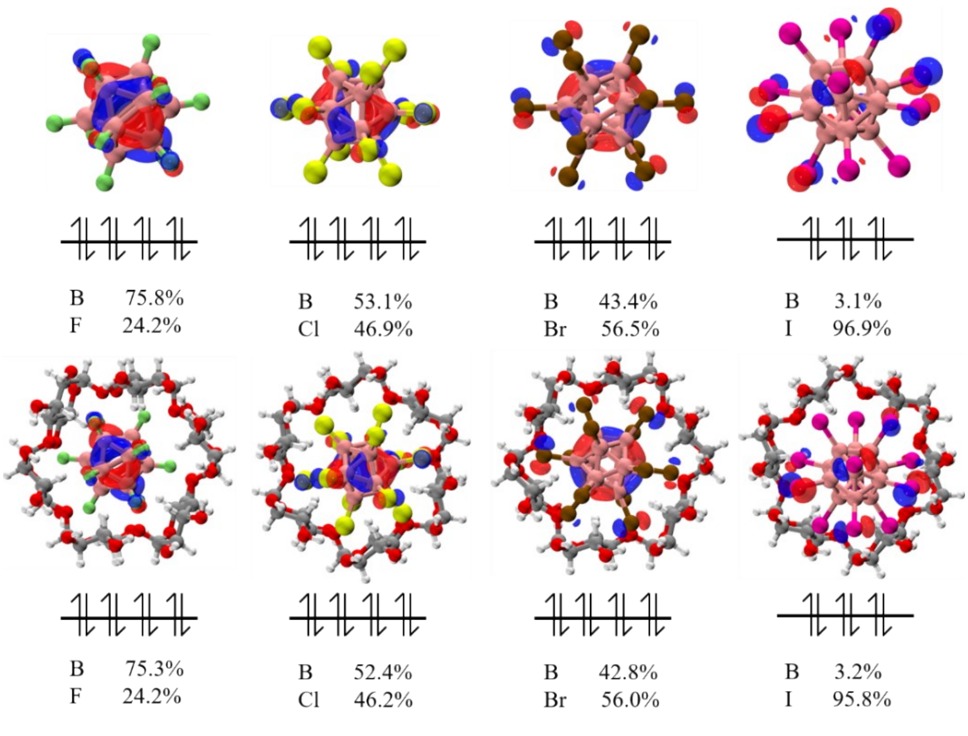

Fig. S7. Plots of highest occupied molecular orbitals (HOMOs) of $B_{12}X_{12}^{2-}$ and α-CD·$B_{12}X_{12}^{2-}$ complexes (isovalue = 0.05 a.u.) and corresponding contribution of fragments to HOMOs at the M06-2X-D3/ma-TZVP level. Note that these complexes clusters possess 3~4 pseudo-degenerate HOMOs (splitting in mean 0.06 eV due to influence of CD) and only one of them is displayed as a representative. The HOMOs of isolated $B_{12}X_{12}^{2-}$ is highly degenerate.

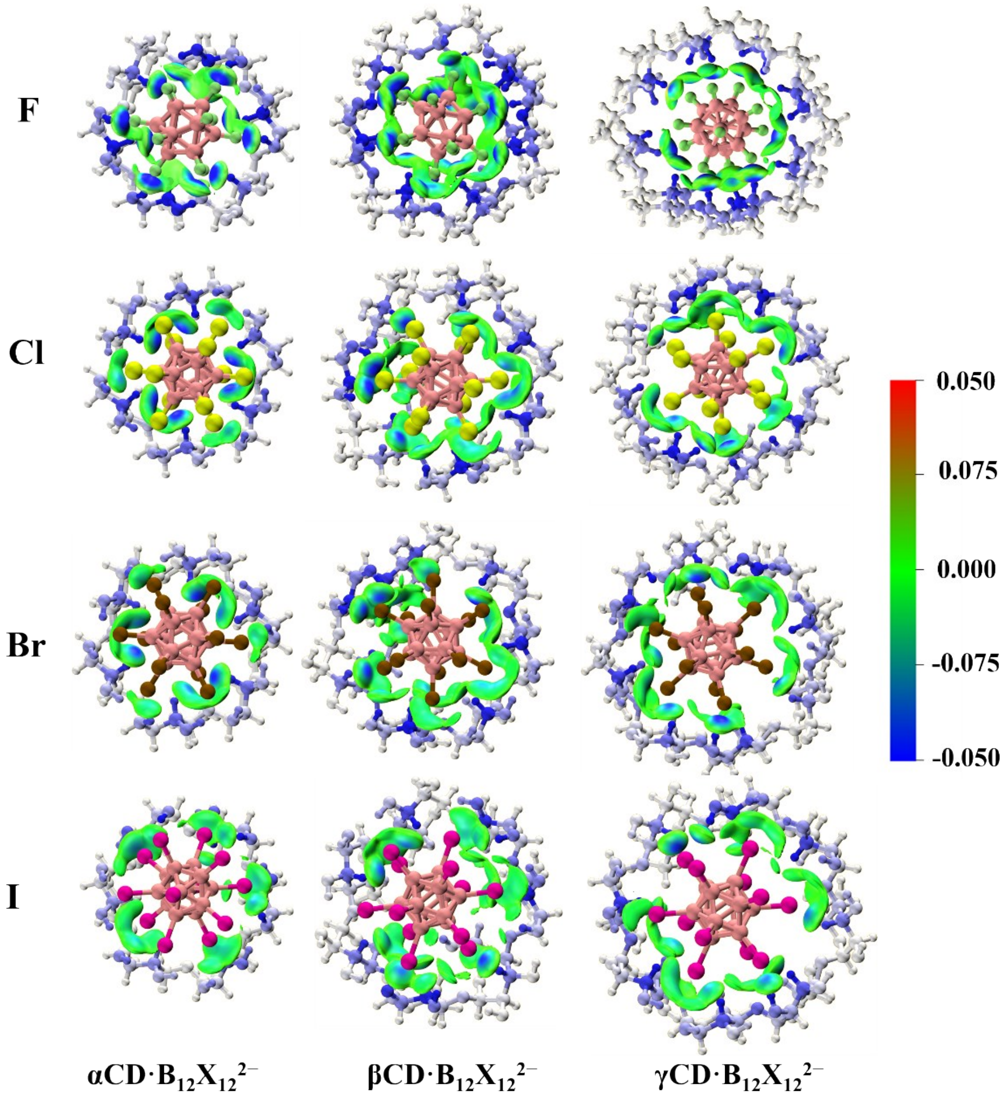

Fig. S8. The δg^{inter} = 0.005 a.u. isosurfaces for CDs·$B_{12}X_{12}^{2-}$ (X = F, Cl, Br, I) colored according to a blue-green-red scheme over the range $-0.05 < \text{sign}(\lambda_2)\rho < 0.05$ a.u., where blue represents the strong electrostatic interaction and green means the weak van der Waals interaction and red indicates the strong repulsion interaction.

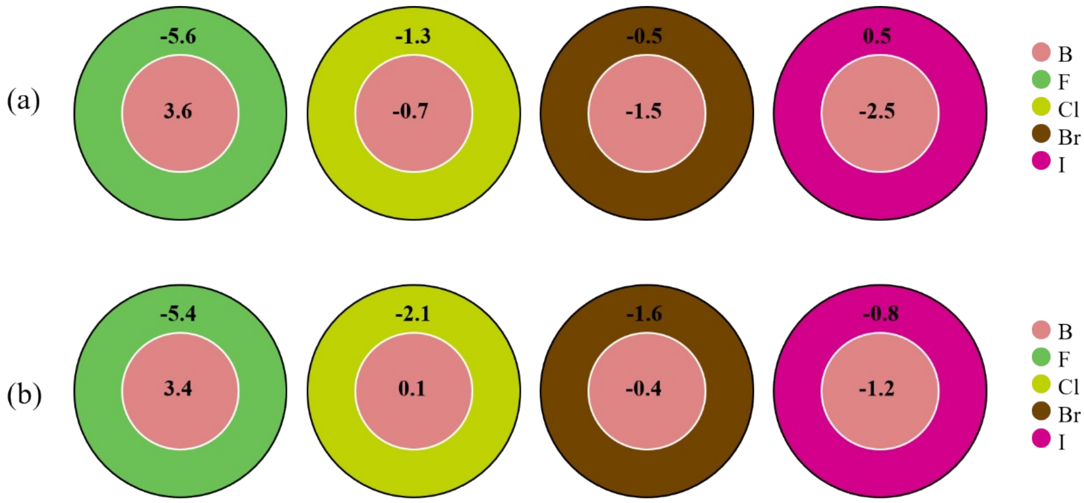

Fig. S9. (a) Calculated natural population analysis charge (NPA charge) and (b) restrained electrostatic potential charge (RESP charge) of $B_{12}X_{12}^{2-}$ (X = F, Cl, Br and I) fragments in $CDs{\cdot}B_{12}X_{12}^{2-}$ complexes at the M06-2X-D3/ma-TZVP level.

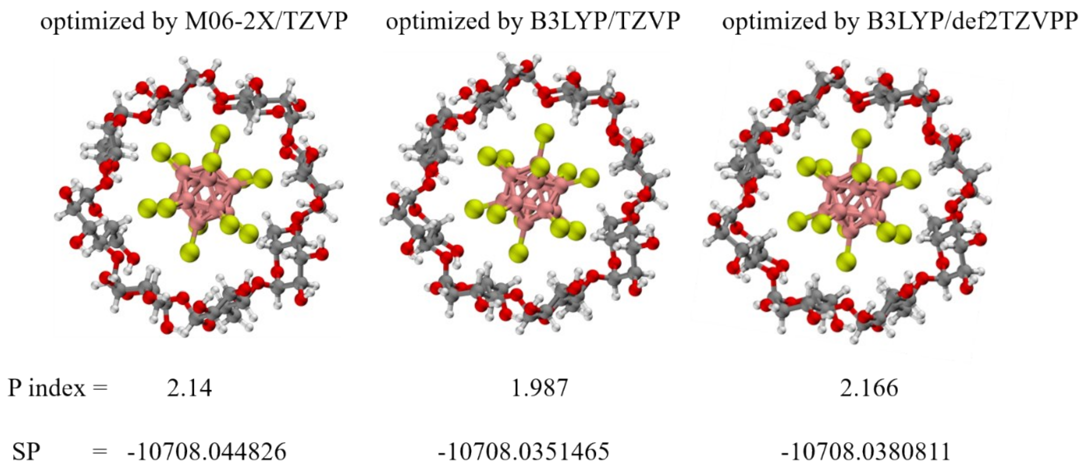

Fig. S10. Geometries of γ-$CD{\cdot}B_{12}Cl_{12}^{2-}$ optimized at M06-2X-D3/TZVP, B3LYP-D3(BJ)/TZVP, and B3LYP-D3(BJ)/def2-TZVPP level. Single point energies were calculated at M06-2X-D3/ma-TZVP level, and the corresponding P index was listed.

Table S1 Calculated VDEs (in eV) for CDs·$B_{12}F_{12}^{2-}$ using different basis set for geometry optimization and single point energy calculation combined at the M06-2X level.

VDE		α-CD·$B_{12}F_{12}^{2-}$		β-CD·$B_{12}F_{12}^{2-}$		γ-CD·$B_{12}F_{12}^{2-}$	
		Basis set for single point energy					
		6-311+G**	ma-TZVP	6-311+G**	ma-TZVP	6-311+G**	ma-TZVP
Basis set for geometry optimization	6-311G**	4.06[a]	3.97	4.76[a]	4.65	4.67[a]	4.56
	TZVP	/	3.89	/	4.59	/	4.35
Expt.		**4.00[a]**		**4.33[a]**		**4.30[a]**	

[a] Numbers from reference 3.

Table S2 (a) Calculated energetics of two conformers for $B_{12}F_{12}^{2-}$ binding with smaller opening of β-CD at the M06-2X-D3/ma-TZVP level. (b) the corresponding molecular structure diagram were also shown.

(a)

Structures	β-CD·$B_{12}F_{12}^{2-}$	Δ/Kcal/mol
	-5773.128978 a.u.	0
smaller opening of β-CD 1	-5773.121204 a.u.	4.8970908
smaller opening of β-CD 2	-5773.121206 a.u.	4.8961836

(b)

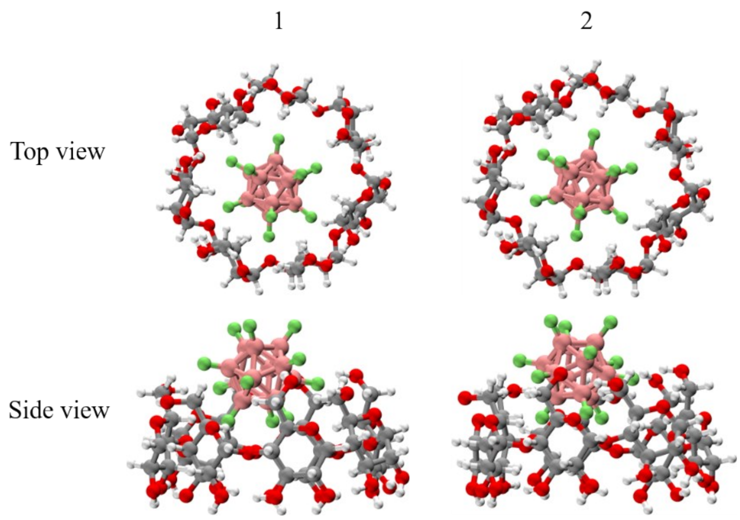

Table S3 The VDEs of CDs·$B_{12}Cl_{12}^{2-}$ at the level of M062X-D3/ma-TZVP based on the structures optimized using TZVP combined with M062X-D3, B3LYP-D3(BJ), and PBE0-D3(BJ), respectively.

VDE/eV	M062X/TZVP-opt	B3LYP/TZVP-opt	PEB0/TZVP-opt	Expt.
α-CD·$B_{12}Cl_{12}^{2-}$	4.24	4.26	4.17	4.09
β-CD·$B_{12}Cl_{12}^{2-}$	4.66	4.70	4.62	4.64
γ-CD·$B_{12}Cl_{12}^{2-}$	4.66	4.72	4.67	4.69

Table S4 The VDEs of αCD·$B_{12}Cl_{12}^{2-}$ employing ma-TZVP combined with M062X-D3, PBE-D3(BJ), B3LYP-D3(BJ), and PBE0-D3(BJ), respectively, based on the structures optimized at the level of M062X-D3/TZVP.

eV	M062X	PBE	B3LYP	PBE0	Expt.
VDE	4.24	3.39	3.69	3.77	4.09

Table S5 The VDEs of CDs·$B_{12}Cl_{12}^{2-}$ at the level of M062X-D3, B3LYP-D3(BJ), PBE0-D3(BJ)/ma-TZVP based on the structures optimized at the level of corresponding functionals with TZVP basis set.

VDE/eV	M062X	B3LYP	PBE0	Exp.
α-CD·$B_{12}Cl_{12}^{2-}$	4.24	3.71	3.71	4.09
β-CD·$B_{12}Cl_{12}^{2-}$	4.66	4.13	4.14	4.64
γ-CD·$B_{12}Cl_{12}^{2-}$	4.66	4.18	4.20	4.69

Table S6 The experimental ΔVDEs between the isolated $B_{12}X_{12}^{2-}$ (X = F, Cl, Br and I) and corresponding CDs·$B_{12}X_{12}^{2-}$ complexes.

ΔVDE/eV	$B_{12}F_{12}^{2-}$	$B_{12}Cl_{12}^{2-}$	$B_{12}Br_{12}^{2-}$	$B_{12}I_{12}^{2-}$
α-CD	2.10	1.14	0.91	0.74
β-CD	2.43	1.69	1.38	1.08
γ-CD	2.40	1.74	1.50	1.25

Table S7 Calculated SP energetics (in kcal/mol) and VDEs (in eV) for the first two lowest-lying structures of α-CD·$B_{12}X_{12}^{2-}$ (X = F, Cl, Br and I) at the M06-2X-D3/ma-TZVP level.

VDE/eV	Exp.	Lowest-lying	Isomer
α-CD·$B_{12}F_{12}^{2-}$	4.00	3.89	3.94
α-CD·$B_{12}Cl_{12}^{2-}$	4.09	4.24	4.22
α-CD·$B_{12}Br_{12}^{2-}$	4.11	4.32	4.31
α-CD·$B_{12}I_{12}^{2-}$	3.54	3.79	3.78
Relative energy/kcal/mol		**Lowest-lying**	**Isomer**
α-CD·$B_{12}F_{12}^{2-}$		0	2.05
α-CD·$B_{12}Cl_{12}^{2-}$		0	1.71
α-CD·$B_{12}Br_{12}^{2-}$		0	2.91
α-CD·$B_{12}I_{12}^{2-}$		0	1.82

Table S8 The contribution of each fragment to HOMOs of CDs·$B_{12}X_{12}^{2-}$ at the M06-2X-D3/ma-TZVP level.

	$B_{12}F_{12}^{2}$		$B_{12}Cl_{12}^{2}$		$B_{12}Br_{12}^{2}$		$B_{12}I_{12}^{2}$	
	B	F	B	Cl	B	Br	B	I
α-CD	75.3%	24.2%	52.4%	46.2%	42.8%	56.0%	3.2%	95.8%
β-CD	56.2%	24.2%	51.7%	46.0%	42.0%	55.2%	3.2%	95.4%
γ-CD	75.4%	24.0%	52.0%	45.7%	42.2%	55.1%	3.1%	94.9%

Table S9 Energy decomposition analysis components (in eV) for CDs·$B_{12}X_{12}^{2-}$ (X = F, Cl, Br and I) performed at the (a) SAPT0/jun-cc-pVDZ (jun-cc-pVDZ-pp for I atom) and (b) canonical EDA using B3LYP-D3(BJ)/TZ2P. The negative values indicate the attractive terms, and positive values indicate the repulsive potential.

(a)

SAPT0	E_exch	E_elstat	E_ind	E_disp	Total
αCD-F	2.21	-2.83	-1.21	-1.19	-3.01
βCD-F	3.41	-4.29	-1.52	-1.97	-4.37
γCD-F	2.12	-3.39	-1.42	-1.48	-4.16
αCD-Cl	1.91	-1.85	-0.73	-1.40	-2.08
βCD-Cl	2.80	-2.94	-1.06	-2.20	-3.40
γCD-Cl	2.66	-2.80	-1.09	-2.21	-3.45
αCD-Br	1.81	-1.69	-0.64	-1.39	-1.91
βCD-Br	3.37	-3.13	-1.03	-2.49	-3.28
γCD-Br	2.85	-2.76	-1.05	-2.40	-3.37
αCD-I	2.23	-1.97	-0.66	-1.59	-1.99

βCD-I	3.43	-3.18	-1.00	-2.49	-3.24
γCD-I	3.30	-2.74	-1.01	-2.65	-3.09

(b)

EDA	ΔE_{Pauli}	ΔV_{elstat}	ΔE_{oi}	ΔE_{disp}	Total
αCD-F	2.34	-2.98	-1.66	-1.05	-3.35
βCD-F	3.69	-4.50	-2.09	-1.70	-4.60
γCD-F	2.28	-3.43	-1.86	-1.36	-4.37
αCD-Cl	1.94	-1.85	-1.10	-1.27	-2.28
βCD-Cl	2.91	-3.00	-1.58	-1.95	-3.62
γCD-Cl	2.77	-2.97	-1.62	-2.00	-3.82
αCD-Br	1.81	-1.75	-1.02	-1.31	-2.26
βCD-Br	3.49	-3.26	-1.65	-2.26	-3.67
γCD-Br	2.95	-2.99	-1.66	-2.26	-3.95
αCD-I	2.25	-2.14	-1.08	-1.57	-2.55
βCD-I	3.52	-3.36	-1.65	-2.36	-3.85
γCD-I	3.35	-2.91	-1.65	-2.59	-3.81

Table S10 (a) Numbers of two types of hydrogen bond, (C-H···X-B) and (O-H···X-B), in CDs·$B_{12}X_{12}^{2-}$ (X = F, Cl, Br and I). The criteria to define a hydrogen bond herein is: (i) within a cutoff distance of 3.9 Å between the donor (C/O in CDs) and acceptor (X in $B_{12}X_{12}^{2-}$) and (ii) the bond angle of (D-H···A) less than 40° counted by VMD code. For example, in β-CD·$B_{12}F_{12}^{2-}$ complex, thirteen C-H···F-B and five O-H···F-B hydrogen bonds are counted. Note that if one X acceptor is shared by two H donors, the hydrogen bonds are counted by twice.

(C-H···X-B)+(O-H···X-B)	$B_{12}F_{12}^{2-}$	$B_{12}Cl_{12}^{2-}$	$B_{12}Br_{12}^{2-}$	$B_{12}I_{12}^{2-}$
α-CD	6+4	3+0	3+0	0+1
β-CD	13+5	6+4	4+3	2+1
γ-CD	10+2	5+3	6+2	2+2

Despite the equivalent numbers of hydrogen bonds of αCD·$B_{12}Cl_{12}^{2-}$ and αCD·$B_{12}Br_{12}^{2-}$, there is a slight advantage in the total binding energies of αCD·$B_{12}Cl_{12}^{2-}$ over that of αCD·$B_{12}Br_{12}^{2-}$ due to the more appropriate size ratio and larger electronegativity of Cl atoms.

(b) Schematic of hydrogen bonds (labeled in blue) in CDs·$B_{12}X_{12}^{2-}$ (X = F, Cl, Br and I) with side and top views.

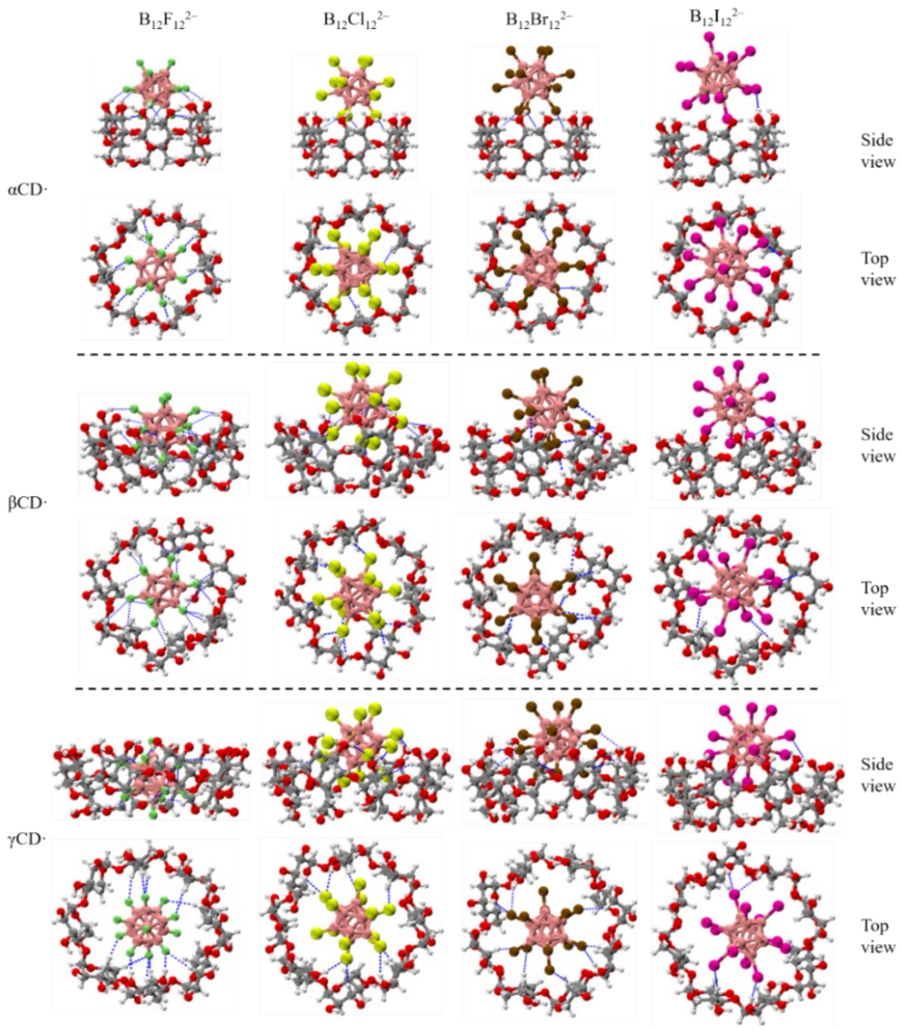

References

(1) BIOVIA, D. S. *Materials Studio*, 17.1.0.48; San Diego: Dassault Systèmes, 2017.
(2) J. Warneke, G.-L. Hou, E. Aprà, C. Jenne, Z. Yang, Z. Qin, K. Kowalski, X.-B. Wang, S. S. Xantheas. *J. Am. Chem. Soc.* 2017, 139, 14749.
(3) Li, Z.; Jiang, Y.; Yuan, Q.; Warneke, J.; Hu, Z.; Yang, Y.; Sun, H.; Sun, Z. and Wang, X.-B. Photoelectron spectroscopy and computational investigations of the electronic structures and noncovalent interactions of cyclodextrin-closo-dodecaborate anion complexes χ-CD·$B_{12}X_{12}^{2-}$ (X = α, β, γ; X = H, F) *Phys. Chem. Chem. Phys.* 2020, 22, 7193-7200.